Applied Catalysis B: Environmental 142–143 (2013) 187–195

Contents lists available at SciVerse ScienceDirect

Applied Catalysis B: Environmental

journal homepage: www.elsevier.com/locate/apcatb

Hydroxyapatite supported ruthenium(0) nanoparticles catalyst in hydrolytic dehydrogenation of ammonia borane: Insight to the nanoparticles formation and hydrogen evolution kinetics

Serdar Akbayrak, Pelin Erdek, Saim Özkar*

Department of Chemistry, Middle East Technical University, 06800 Ankara, Turkey

ARTICLE INFO

Article history:
Received 31 March 2013
Received in revised form 2 May 2013
Accepted 8 May 2013
Available online 15 May 2013

Keywords:
Ruthenium nanoparticles
Hydroxyapatite
Heterogenous catalyst
Hydrolysis
Ammonia borane

ABSTRACT

When a solution of ammonia borane is added to the suspension of ruthenium(III) ions supported on hydroxyapatite, both reduction of ruthenium(III) to ruthenium(0) nanoparticles and hydrogen release from the hydrolysis of ammonia borane occur concomitantly at room temperature. Using the hydrogen evolution from the hydrolysis of ammonia borane as reporter reaction provides valuable insights to the formation kinetics of ruthenium(0) nanoparticles. Thus, the rate constants for the slow nucleation and autocatalytic surface growth of ruthenium(0) nanoparticles could be obtained. Furthermore, the evaluation of rate constants at various temperatures provides the estimation of activation energies for both reactions; $E_a = 166 \pm 7$ kJ/mol for the nucleation and $E_a = 59 \pm 2$ kJ/mol for the autocatalytic surface growth of ruthenium(0) nanoparticles. The ruthenium(0) nanoparticles, in situ formed during the hydrolysis of ammonia borane and supported on hydroxyapatite, could be isolated from the reaction solution and characterized by a combination of advanced analytical techniques. The results show that (i) highly dispersed ruthenium(0) nanoparticles of 4.7 ± 0.7 nm size were formed on the surface of hydroxyapatite, (ii) they are highly active catalyst in the hydrolytic dehydrogenation of ammonia borane with a turnover frequency value of 137 min^{-1} at 25.0 ± 0.1 °C, and (iii) they are long lived and reusable catalyst providing 87,000 turnovers for hydrogen generation from the hydrolysis of ammonia borane and preserving 92% of their initial catalytic activity even after the fifth run of hydrolysis of ammonia borane at 25.0 ± 0.1 °C. The results of kinetic study on the hydrogen generation from the hydrolysis of ammonia borane were also reported including the activation energy of 58 ± 2 kJ/mol for the hydrolytic dehydrogenation of ammonia borane.

1. Introduction

The use of hydrogen as energy carrier is anticipated to facilitate the transition from fossil fuels to the renewable energy sources, on the way towards a sustainable energy future [1]. However, safe and compact storage of hydrogen is still the key issue in hydrogen economy [2,3]. Consequently, there has been extensive motivation in searching for chemical materials possessing high gravimetric hydrogen density suitable for both portable and stationary applications of hydrogen supply [4]. Many chemical hydrides have been tested as hydrogen storage materials for onboard applications [5–11]. Recent reports [12–19] have shown that B–N adducts need to be considered as hydrogen storage materials because of their high content of hydrogen with multiple nature, the protic N–H and hydridic B–H hydrogen [20]. Ammonia borane (AB, NH_3BH_3) is a leading candidate as hydrogen storage medium because of its high stability, nontoxicity and potential capacity of 19.6 wt.% H_2 [21,22], one of the highest hydrogen density materials [23]. Hydrogen stored in AB can be released by thermal dehydrogenation [24], methanolysis [25] or hydrolysis [26]. As the thermal dehydrogenation requires high temperature, solvolysis appears to be favorable for hydrogen generation from AB at low temperature. However, AB is relatively stable to hydrolysis in aqueous solution [12]. Therefore, the hydrolytic dehydrogenation of AB occurs at an appreciable rate only in the presence of suitable catalyst at room temperature (Eq. (1)).

$$H_3NBH_3(aq) + 2H_2O(l) \xrightarrow{\text{catalyst}} NH_4^+(aq) + BO_2^-(aq) + 3H_2(g) \quad (1)$$

A wealth of new reports on the hydrogen release from AB has been published using transition metal nanoparticles as catalysts [23,26–31]. However, transition metal nanoparticles tend to aggregate into clumps causing a decrease in catalytic activity [32,33]. An efficient way of preventing the aggregation of metal nanoparticles is to use supporting materials such as zeolites [34,35], carbon

* Corresponding author. Tel.: +90 312 210 3212; fax: +90 312 210 3200.
E-mail address: sozkar@metu.edu.tr (S. Özkar).

0926-3373/$ – see front matter © 2013 Elsevier B.V. All rights reserved.
http://dx.doi.org/10.1016/j.apcatb.2013.05.015

nanotubes [36], graphenes [37], hydroxyapatites [38] and polymers [39]. Hydroxyapatites have attracted great interest as a catalyst support due to their high ion exchange ability, high adsorption capacity and nonporous structures that reduce the mass transfer limitations [40]. Herein, we report the in situ generation of ruthenium(0) nanoparticles supported on hydroxyapatite, Ru(0)@HAp, during the hydrolysis of AB. Ru(0)@HAp were prepared by the ion-exchange of Ru^{3+} ions with Ca^{2+} ions in the lattice of HAp and then reduced by AB at room temperature. Ru(0)@HAp were isolated from the reaction solution and characterized by ICP-OES, XRD, TEM, SEM, EDX and XPS techniques. Our report also includes the following major findings: (i) Highly dispersed ruthenium(0) nanoparticles were formed on the surface of hydroxyapatite with particle size in the range 3.0–5.5 nm. (ii) Monitoring the hydrogen evolution from the hydrolysis of AB gave some valuable insights into the kinetics of nanoparticles formation. (iii) Ru(0)@HAp are long lived catalyst with a total turnover number of 87,000 in hydrogen generation from the hydrolysis of AB at room temperature. (iv) Ru(0)@HAp are also reusable catalysts as they retain 92% of the initial catalytic activity in the hydrolytic dehydrogenation of ammonia borane even after the fifth run of hydrolysis.

2. Experimental

2.1. Materials

Ruthenium(III) chloride trihydrate ($RuCl_3{\cdot}3H_2O$), ammonia borane (AB, 97%) and hydroxyapatite were purchased from Aldrich. Deionized water was distilled by water purification system (Milli-Q System). All glassware and Teflon-coated magnetic stir bars were cleaned with acetone, followed by copious rinsing with distilled water before drying in an oven at 150 °C.

2.2. Characterization

The ruthenium contents of the Ru(0)@HAp samples were determined by Inductively Coupled Plasma Optical Emission Spectroscopy (ICP-OES, Leeman-Direct Reading Echelle) after each sample was completely dissolved in the mixture of HNO_3/HCl (1/3 ratio). Transmission electron microscopy (TEM) was performed on a JEM-2100F (JEOL) microscope operating at 200 kV. A small amount of powder sample was placed on the holey carbon grid of the transmission electron microscope. Samples were examined at magnification between 100 and 400 K. Scanning electron microscope (SEM) images were taken using a JEOL JSM-5310LV at 15 kV and 33 Pa in a low-vacuum mode without metal coating on aluminum support. The X-ray photoelectron spectroscopy (XPS) analysis was performed on a Physical Electronics 5800 spectrometer equipped with a hemispherical analyzer and using monochromatic Al Kα radiation of 1486.6 eV, the X-ray tube working at 15 kV, 350 W and pass energy of 23.5 keV. ^{11}B NMR spectra were recorded on a Bruker Avance DPX 400 with an operating frequency of 128.15 MHz for ^{11}B.

2.3. Preparation of ruthenium(III) exchanged hydroxyapatite (Ru(III)@HAp)

Hydroxyapatite (500 mg) was added to a solution of $RuCl_3{\cdot}xH_2O$ (57.7 mg) in 100 mL H_2O in a 250 mL round bottom flask. This slurry was stirred at room temperature for three days. The Ru(III)@HAp sample was filtered by using Whatman-1 filter paper, washed with 100 mL of distilled water and the remnant was dried under vacuum (10^{-3} Torr) at 80 °C.

2.4. In situ formation of ruthenium(0) nanoparticles supported on hydroxyapatite (Ru(0)@HAp) and concomitant catalytic hydrolytic dehydrogenation of AB

Ruthenium(0) nanoparticles supported on hydroxyapatite were in situ generated from the reduction of Ru(III)@HAp during the catalytic hydrolysis of AB. Before starting the catalyst formation and concomitant catalytic hydrolysis of AB, a jacketed reaction flask (20 mL) containing a Teflon-coated stir bar was placed on a magnetic stirrer (Heidolph MR-301) and thermostated to 25.0 ± 0.1 °C by circulating water through its jacket from a constant temperature bath. Then, a graduated glass tube (60 cm in height and 3.0 cm in diameter) filled with water was connected to the reaction flask to measure the volume of the hydrogen gas to be evolved from the reaction. Next, 10 mg powder of Ru(III)@ HAp (3.96 wt.% Ru) was dispersed in 10 mL distilled water in the reaction flask thermostated at 25.0 ± 0.1 °C. Then, 31.8 mg AB (1.0 mmol $H_3N{\cdot}BH_3$) was added into the flask and the reaction medium was stirred at 1000 rpm. After a short induction period of less than 6.0 min, ruthenium(0) nanoparticles were formed and the catalytic hydrolysis of AB started. The volume of hydrogen gas evolved was measured by recording the displacement of water level every 30 s at constant atmospheric pressure of 693 Torr. The reaction was stopped when no more hydrogen evolution was observed. In each experiment, the resulting solutions were filtered and the filtrates were analyzed by ^{11}B NMR and conversion of AB to metaborate anion was confirmed by comparing the intensity of signals in the ^{11}B NMR spectra of the filtrates.

2.5. Determination of the most active ruthenium loading for Ru(0)@HAp used in the hydrolytic dehydrogenation of AB

The catalytic activity of Ru(0)@HAp samples with various ruthenium loading in the range of 1.0–8.0 wt.% was tested in hydrogen generation from the hydrolysis of AB starting with 0.784 mM Ru and 100 mM AB in 10 mL solution at 25 ± 0.1 °C. The highest catalytic activity was achieved by using 3.96 wt.%. ruthenium loaded hydroxyapatite. For all the tests reported hereafter, ruthenium loading of 3.96 wt.% was used unless otherwise stated.

2.6. Determination of activation energy for hydrolytic dehydrogenation of AB catalyzed by Ru(0)@HAp

In a typical experiment, the hydrolysis reaction was performed starting with 10 mL of 100 mM (31.8 mg) AB solution and 10 mg Ru(III)@HAp (3.96 wt.% ruthenium, [Ru] = 0.392 mM) at various temperatures (20, 25, 30, 35, 40 °C) in order to obtain the activation energy.

2.7. Reusability of Ru(0)@HAp in the hydrolytic dehydrogenation of AB

After the complete hydrolysis of AB started with 10 mL of 100 mM AB (31.8 mg H_3NBH_3), and 30 mg Ru(III)@HAp (3.96 wt.% ruthenium, [Ru] = 1.175 mM) at 25 ± 0.1 °C, the catalyst was isolated as dark-grey powder by centrifugation and dried under vacuum (10^{-3} Torr) at 80 °C after washing with 100 mL of water. The isolated samples of Ru(0)@HAp were weighed and redispersed in 10 mL solution of 100 mM AB for a subsequent run of hydrolysis at 25 ± 0.1 °C.

2.8. Determination of the catalytic lifetime of Ru(0)@HAp in the hydrolytic dehydrogenation of AB

The catalytic lifetime of Ru(0)@HAp in the hydrolysis of AB was determined by measuring the total turnover number (TTO). Such a

lifetime experiment was started with a 100 mL solution containing 0.784 mM Ru(0)@HAp and 30 mM AB at 25.0 ± 0.1 °C. When all the ammonia borane present in the solution was completely hydrolyzed, more AB was added and the reaction was continued in this way until no hydrogen gas evolution was observed.

3. Results and discussion

3.1. Formation kinetics of ruthenium(0) nanoparticles catalyst during the hydrolytic dehydrogenation of AB

Ruthenium(0) nanoparticles supported on hydroxyapatite were in situ generated during the hydrolysis of ammonia borane. Ru(0)@HAp are prepared by the ion-exchange of Ru^{3+} ions with Ca^{2+} ions in the lattice of HAp and then reduced by AB at room temperature. When AB solution is added to the suspension of hydoxyapatite containing ruthenium(III) ions, both reduction of ruthenium(III) to ruthenium(0) and hydrogen release from the hydrolysis of AB occur concomitantly. The progress of ruthenium(0) nanoparticles formation and concomitant hydrolytic dehydrogenation of ammonia borane was followed by monitoring the change in H_2 pressure which was then converted into the equivalent H_2 per mole of AB, using the known 3:1 H_2/AB stoichiometry (Eq. (1)).

Fig. 1 shows the evolution of equivalent hydrogen per mole of AB versus time plot for the hydrolytic dehydrogenation of AB starting with Ru(III)@HAp precatalyst (0.196 mM Ru) and 100 mM AB at 25 ± 0.1 °C. After a short induction period of 6.0 min the hydrogen generation starts and continues almost linearly until the release of 3.0 equivalents H_2 per mole of AB. Note that the amount of H_2 released from the reduction of ruthenium(III) to ruthenium(0) is negligible compared to that evolved from the hydrolysis of ammonia borane as the molar ratio of AB to Ru is greater than 500. The observation of an induction period and a sigmoidal shape of dehydrogenation curve indicates the formation of ruthenium(0) nanoparticles with a 2-step, nucleation and autocatalytic growth mechanism [41,42]. The formation kinetics of the ruthenium(0) nanoparticles catalyst can be obtained using the hydrolytic dehydrogenation of AB as reporter reaction [41–43], given in Scheme 1 whereby P is the precursor ruthenium(III) ion-exchanged into hydroxyapatite and Q is the growing $Ru(0)_n$ nanoparticles.

The hydrolytic dehydrogenation of AB will accurately report on and amplifies the amount of $Ru(0)_n$ nanoparticles catalyst, Q, present if the hydrogen generation rate is fast in comparison to the rate of nanoparticle formation. It was shown that the hydrolytic

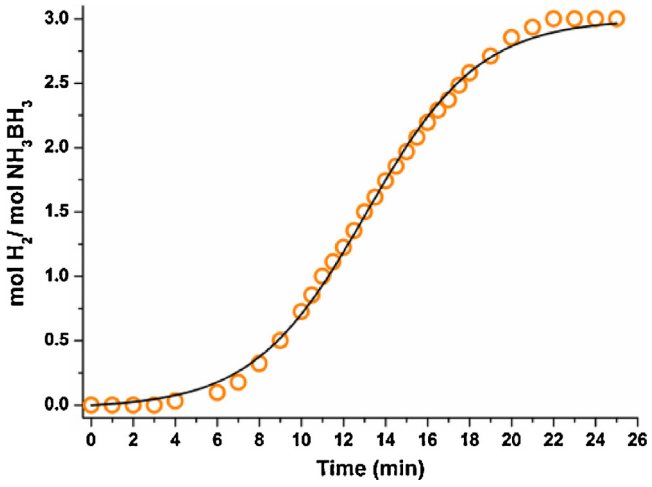

Fig. 1. The evolution of equivalent H_2 per mole of AB versus time plot for the hydrolytic dehydrogenation of AB starting with Ru(III)@HAp precatalyst (0.196 mM Ru) and 100 mM AB at 25 ± 0.1 °C.

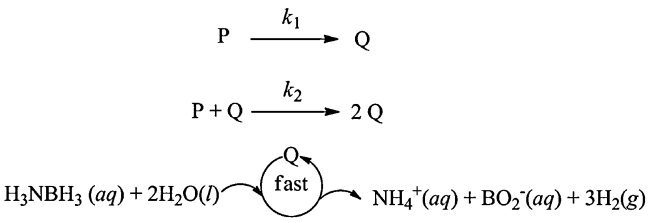

Scheme 1. Illustration of the hydrolytic dehydrogenation of ammonia borane as reporter reaction: P is the precursor ruthenium(III) ion-exchanged into hydroxyapatite and Q is the growing $Ru(0)_n$ nanoparticles catalyst.

dehydrogenation is zero-order in [AB] when the substrate to catalyst ratio is large enough to ensure that the dehydrogenation reporter reaction is fast relative to the rate of slower nanoparticle formation k_1 and k_2 steps (Scheme 1). Sigmoidal kinetics can be seen in Fig. 1, and fit well by the Finke–Watzky 2-step, nucleation and autocatalytic growth mechanism of nanoparticle formation [43]. The observation of a sigmoidal dehydrogenation curve and its curve-fit to the slow, continuous nucleation, P → Q (rate constant k_1) followed by autocatalytic surface growth, P + Q → 2Q (rate constant k_2) kinetics are very strong evidence for the formation of metal(0) nanoparticles catalyst from a soluble transition-metal complex in the presence of reducing agent [43]. The rate constants determined from the nonlinear least squares curve-fit in Fig. 1 are $k_1 = 4.67 \times 10^{-5} \pm 4.0 \times 10^{-6}\ s^{-1}$ and $k_2 = 1.05 \pm 2.0 \times 10^{-2}\ M^{-1}\ s^{-1}$ (the mathematically required correction has been made to k_2 for the stoichiometry factor of 510 as described elsewhere [42], but not for the "scaling factor"; that is, no correction has been made for changing the number of ruthenium atoms on the growing metal surface). These rate constants are for the continuous slow nucleation and autocatalytic growth reaction of $Ru(0)_n$ nanoparticles, respectively, starting with Ru(III)@HAp precatalyst (0.196 mM Ru) and ammonia borane (100 mM) in aqueous solution at 25 ± 0.1 °C. Note that there exists no direct correlation between the k_1 and k_2 values as they are the rate constants of two different reactions.

Since monitoring the reporter reaction enables us to follow the kinetics of nanoparticle formation, we have carried out the same nanoparticle formation experiment at various temperature in order to estimate the activation energies for the nucleation and autocatalytic surface growth of ruthenium(0) nanoparticles catalyst. Fig. 2a shows the evolution of equivalent hydrogen per mole of AB versus time plot for the hydrolytic dehydrogenation of AB starting with Ru(III)@HAp precatalyst (0.392 mM Ru) and 100 mM at five different temperatures. For each temperature, experimental data curve-fit well to the two-step mechanism, giving the rate constants k_1 of the slow, continuous nucleation, P → Q, and k_2 of the autocatalytic surface growth, P + Q → 2Q for the formation of ruthenium(0) nanoparticles catalyst from the ruthenium(III) ions during the hydrolysis of ammonia borane (Table 1) [43]. The large value of k_2/k_1 ratio also given in Table 1 is indicative of the high level kinetic control in the formation of ruthenium(0) nanoparticles from the reduction of the precursor ruthenium(III) ions on the surface of hydroxyapatite [43]. From the Arrhenius plots

Table 1
The rate constants k_1 of the slow, continuous nucleation, P → Q, and k_2 of the autocatalytic surface growth, P + Q → 2Q for the formation of ruthenium(0) nanoparticles catalyst from the reduction of ruthenium(III) ions during the hydrolysis of AB at various temperatures.

Temperature (°C)	k_1 (s^{-1})	k_2 ($M^{-1}s^{-1}$)	k_2/k_1
20	$5.83 \times 10^{-6} \pm 7.4 \times 10^{-7}$	$0.655 \pm 1.3 \times 10^{-2}$	1.12×10^3
25	$2.37 \times 10^{-5} \pm 3.3 \times 10^{-6}$	$0.888 \pm 2.4 \times 10^{-2}$	3.75×10^3
30	$1.05 \times 10^{-5} \pm 2.3 \times 10^{-6}$	$1.49 \pm 4.8 \times 10^{-2}$	1.42×10^3
35	$7.85 \times 10^{-5} \pm 1.3 \times 10^{-5}$	$2.02 \pm 6.9 \times 10^{-2}$	0.26×10^3
40	$5.01 \times 10^{-4} \pm 6.8 \times 10^{-5}$	$2.43 \pm 1.0 \times 10^{-1}$	0.49×10^3

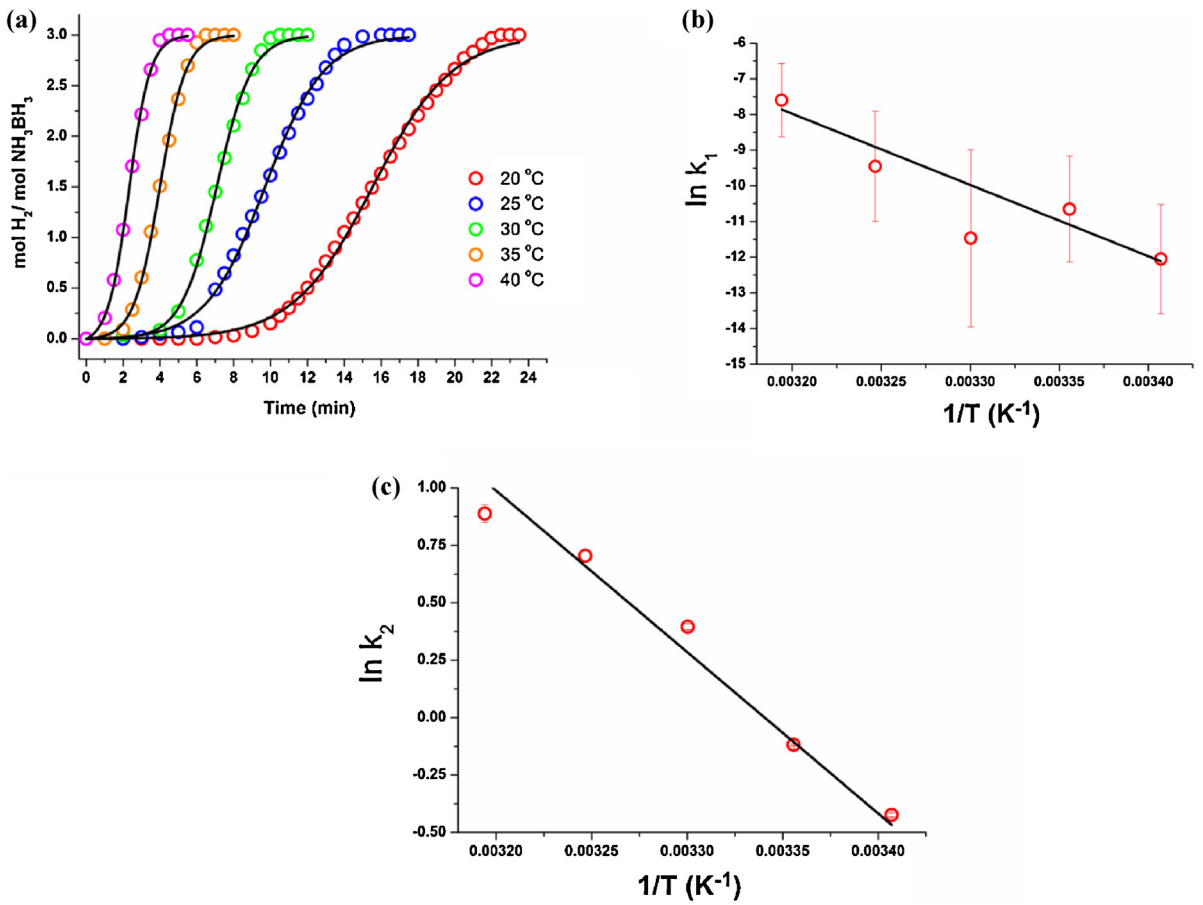

Fig. 2. (a) The evolution of equivalent hydrogen per mole of AB versus time plot for the hydrolytic dehydrogenation of AB starting with Ru(III)@HAp precatalyst (0.392 mM Ru) and 100 mM AB at various temperatures. (b) The Arrhenius plot for nucleation of ruthenium(0) nanoparticles (In $k_1 = -19{,}982.7(1/T) + 55.97$). (c) The Arrhenius plot for the autocatalytic surface growth of ruthenium(0) nanoparticles (In $k_2 = -7024.02(1/T) + 23.46$).

constructed by using the values of rate constants k_1 and k_2 at various temperatures in Fig. 2b and c, one can obtain the activation energy $E_a = 166 \pm 7$ kJ/mol for the nucleation and $E_a = 59 \pm 2$ kJ/mol for the autocatalytic surface growth of ruthenium(0) nanoparticles, respectively. It is noteworthy that the k_1 values have much higher uncertainty compared to the k_2 values. For the first time, the activation energy values for the formation of metal(0) nanoparticles have been estimated from the kinetic data. They give an idea on the energy barrier for the slow nucleation and autocatalytic surface growth of metal(0) nanoparticles catalyst.

3.2. *Isolation and characterization of ruthenium(0) nanoparticles supported on hydroxyapatite*

The ruthenium(0) nanoparticles supported on hydroxyapatite (Ru(0)@HAp), in situ formed during the hydrolysis of AB, could be isolated from the reaction solution as powder by filtration and characterized by ICP-OES, XRD, SEM, EDX, TEM and XPS techniques. Ruthenium content of Ru(0)@HAp was determined by ICP-OES. The comparison of the XRD patterns of hydroxyapatite and Ru(0)@HAp with a ruthenium loading of 3.96 wt.% Ru, given in Fig. 3a and b, respectively, clearly shows that there is no change in the characteristic diffraction peaks of hydroxyapatite. This observation indicates that the host material remains intact after ion-exchange and reduction of ruthenium(III) ions without noticeable alteration in the framework lattice or loss in the crystallinity [44]. There is no observable peak attributable to ruthenium nanoparticles in Fig. 3b, probably as a result of low ruthenium loading of hydroxyapatite.

Fig. 4 exhibits the SEM image and SEM-EDX spectrum of Ru(0)@HAp with a ruthenium loading of 3.96 wt.% indicating that ruthenium is the only element detected in the sample in addition to the framework elements of hydroxyapatite (Ca, P, O).

Fig. 5 shows the TEM images of Ru(0)@HAp with a ruthenium loading of 3.96 wt.% taken with different magnifications, which indicate that (i) highly dispersed ruthenium(0) nanoparticles are formed on the surface of hydroxyapatite with particle size in the range 3.0–5.5 nm (mean diameter: 4.7 ± 0.7 nm, histogram in

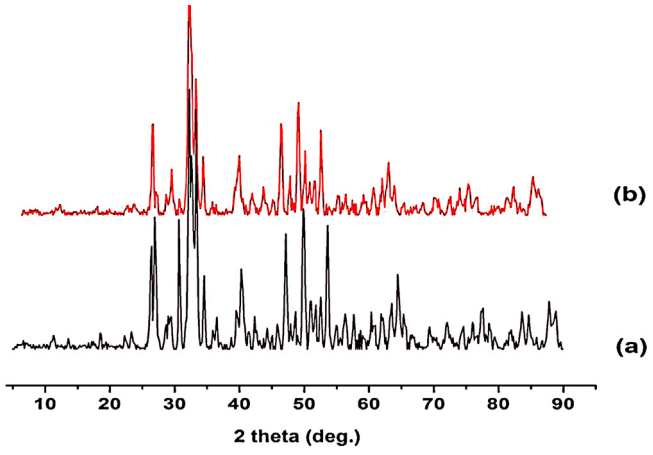

Fig. 3. Powder XRD patterns of (a) hydroxapatite and (b) Ru(0)@HAp with a 3.96 wt.% Ru loading.

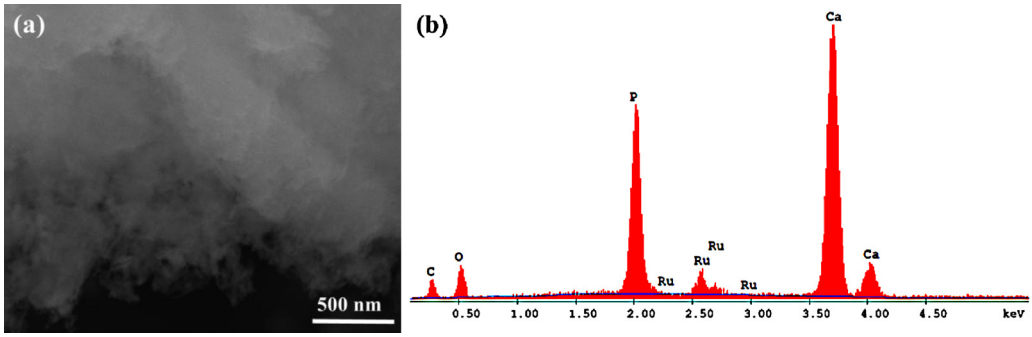

Fig. 4. (a) SEM image (the scale bar is 500 nm) and (b) SEM-EDX spectrum of Ru(0)@HAp with a 3.96 wt.% Ru loading.

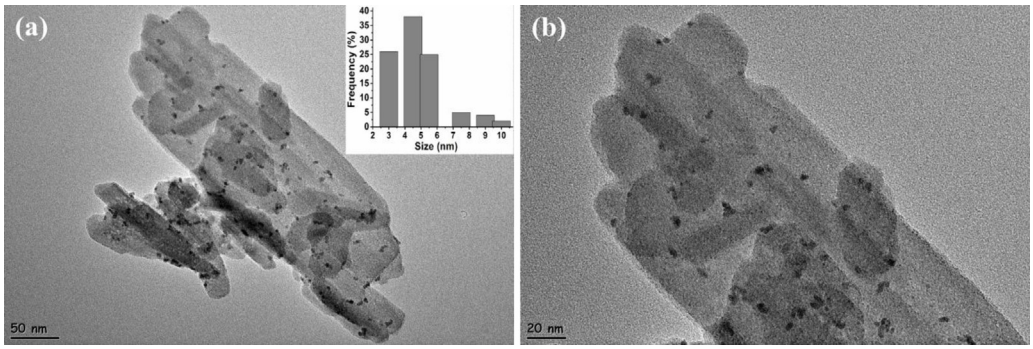

Fig. 5. TEM images of Ru(0)@HAp with a 3.96 wt.% Ru loading in different magnifications with the scale bar of (a) 50 nm and (b) 20 nm and inset: the corresponding histogram for the particle size distribution.

Fig. 5a, inset) and (ii) ion-exchange of ruthenium(III) followed by reduction to ruthenium(0) causes no change in the framework lattice of the hydroxyapatite in agreement with the XRD results.

The composition of Ru(0)@HAp formed in situ during the hydrolysis of AB and the oxidation state of ruthenium were also studied by XPS technique. The survey-scan XPS spectrum of Ru(0)@HAp with a ruthenium loading of 3.96 wt.% (Fig. 6) shows that ruthenium is the only element detected in addition to the hydroxyapatite framework elements (Ca, P, O) in agreement with the SEM-EDX result. High resolution X-ray photoelectron spectrum of a Ru(0)@HAp sample given in the inset of Fig. 6 shows two prominent bands at 284.8 eV and 280.6 eV which can readily be assigned to Ru(0) $3d_{3/2}$ and $3d_{5/2}$, respectively, in the nanoparticles by comparing with the values of ruthenium metal 285 and 280 eV, respectively [45]. It is noteworthy that the Ru(0) $3d_{3/2}$ peak at 284.8 eV overlaps with the C 1 s peak at 284.0 eV coming from air with a percent atomic ratio of 9.29 (C 1 s/Ru 3*d*).

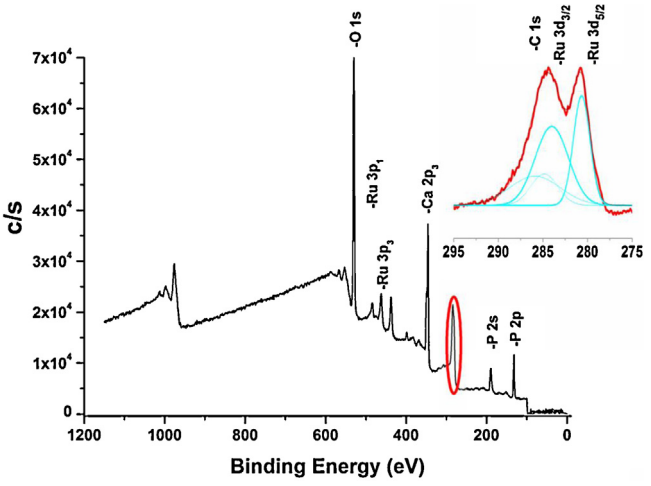

Fig. 6. X-ray photoelectron (XPS) spectrum of Ru(0)@HAp sample with ruthenium loading of 3.96 wt.% Ru. The inset gives the high resolution scan and deconvolution of Ru 3d bands.

3.3. Hydrolytic dehydrogenation of ammonia borane catalyzed by ruthenium(0) nanoparticles supported on hydroxyapatite

A control experiment was performed to check whether hydroxyapatites show any catalytic activity in the hydrolysis of AB before starting the investigation on the catalytic activity of Ru(0)@HAp. In a control experiment starting with 1.0 mmol AB and 10 mg powder of hydroxyapatite (the same amount as the one used in catalytic activity tests) in 10 mL water at 25.0 ± 0.1 °C or 40.0 ± 0.1 °C, no hydrogen generation was observed in 1 h at both temperatures. This observation indicates that the hydrolysis of AB does not occur in the presence of hydroxyapatite in the temperature range used in this study.

Ruthenium(0) nanoparticles supported on hydroxyapatite, Ru(0)@HAp, are found to be highly active catalyst in the hydrolysis of ammonia borane generating 3.0 equivalent H_2 gas per mol of AB in the same temperature range. Expectedly, the catalytic activity depends on the ruthenium loading of catalyst materials. A series of experiments were performed starting with 10 mL solution of 100 mM AB and 0.784 mM Ru using Ru(III)@HAp sample with various ruthenium loading (1.00, 2.00, 2.93, 3.96, 7.90 wt.% Ru) in appropriate amount to provide the same ruthenium concentration in all of the experiments. Fig. 7 shows the evolution of equivalent hydrogen per mole of AB versus time plot for the hydrolytic dehydrogenation of AB (100 mM) starting with Ru(III)@HAp precatalyst (0.784 mM Ru) with different ruthenium loading at 25.0 ± 0.1 °C. All the plots in Fig. 7 curve-fit well to the two-step mechanism, giving the rate constants k_1 of the slow, continuous nucleation, P → Q,

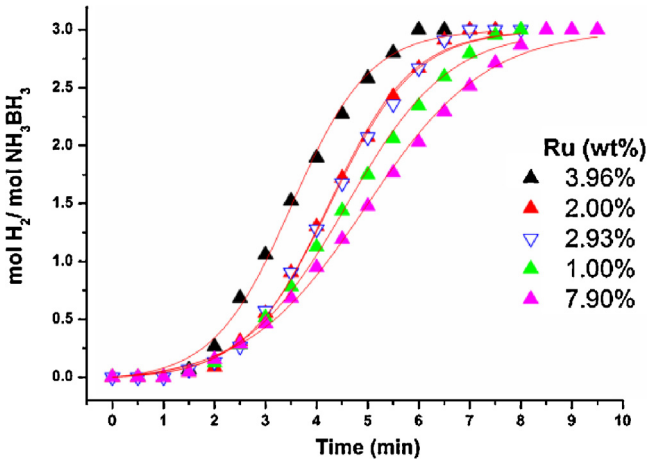

Fig. 7. Plot of mol H_2/mol $H_3N{\cdot}BH_3$ versus time for the hydrolytic dehydrogenation of AB (100 mM) starting with Ru(III)@HAp precatalyst (0.784 mM Ru) with different ruthenium loading at 25.0 ± 0.1 °C.

Table 2
The rate constants k_1 of the slow, continuous nucleation, P → Q, and k_2 of the autocatalytic surface growth, P + Q → 2Q for the formation of ruthenium(0) nanoparticles catalyst from the ruthenium(III) ions during the hydrolysis of AB (100 mM) starting with Ru(0)@HAp with different ruthenium loading (0.784 mM Ru) and the turnover frequency (TOF) of hydrogen generation from the catalytic hydrolysis of AB at 25.0 ± 0.1 °C.

Ru loading of HAp (wt.% Ru)	k_1 (s^{-1})	k_2 ($M^{-1}s^{-1}$)	TOF (min^{-1})
1.00	$1.72 \times 10^{-4} \pm 2.2 \times 10^{-5}$	$0.698 \pm 2.5 \times 10^{-2}$	83
2.00	$1.13 \times 10^{-4} \pm 1.6 \times 10^{-5}$	$0.863 \pm 2.9 \times 10^{-2}$	118
2.93	$1.19 \times 10^{-4} \pm 1.8 \times 10^{-5}$	$0.847 \pm 3.0 \times 10^{-2}$	112
3.96	$2.20 \times 10^{-4} \pm 3.7 \times 10^{-5}$	$0.915 \pm 4.2 \times 10^{-2}$	123
7.90	$2.01 \times 10^{-4} \pm 2.4 \times 10^{-5}$	$0.596 \pm 2.1 \times 10^{-2}$	84

and k_2 of the autocatalytic surface growth, P + Q → 2Q for the formation of ruthenium(0) nanoparticles catalyst from the ruthenium(III) ions during the hydrolysis of ammonia borane (Table 2) [43]. The catalytic activity of in situ generated Ru(0)@HAp, measured as turnover frequency (TOF) in the hydrolytic dehydrogenation of AB at 25.0 ± 0.1 °C, shows variation with the ruthenium loading (Table 2). The Ru(0)@HAp sample with ruthenium loading of 3.96 wt.% Ru provides the highest catalytic activity in hydrogen generation from the hydrolysis of AB at 25.0 ± 0.1 °C. Therefore, Ru(0)@HAp catalyst with ruthenium loading of 3.96 wt.% was used in all of the further experiments performed in this study. It is also noteworthy that the generation of ammonia was checked during the hydrolysis of AB in all the experiments performed in this study following the procedure described elsewhere [46] and no ammonia generation was detected in any of the experiments.

Table 3
The rate constants k_1 of the slow, continuous nucleation, P → Q, and k_2 of the autocatalytic surface growth, P + Q → 2Q for the formation of ruthenium(0) nanoparticles catalyst from the ruthenium(III) ions during the hydrolysis of AB at various concentration of ruthenium.

[Ru] (mM)	k_1 (s^{-1})	k_2 ($M^{-1}s^{-1}$)
0.196	$4.67 \times 10^{-5} \pm 4.0 \times 10^{-6}$	$1.05 \pm 2.2 \times 10^{-2}$
0.392	$2.33 \times 10^{-5} \pm 3.3 \times 10^{-6}$	$0.89 \pm 2.4 \times 10^{-2}$
0.784	$4.62 \times 10^{-6} \pm 9.8 \times 10^{-7}$	$0.72 \pm 2.1 \times 10^{-2}$
1.176	$4.57 \times 10^{-5} \pm 5.3 \times 10^{-6}$	$0.53 \pm 1.2 \times 10^{-2}$

Fig. 8a shows the plots of equivalent H_2 gas generated per mole of H_3NBH_3 versus time during the catalytic hydrolysis of 100 mM AB solution using Ru(0)@HAp with a loading of 3.96 wt.% Ru in different catalyst concentration at 25.0 ± 0.1 °C. In each experiment, hydrogen evolution starts after a short induction period of less than 6 minutes and continues almost linearly until the complete conversion of the substrate giving 3.0 equivalents of H_2 per mole of AB. All the experimental data fit well to sigmoidal curve according to the two-step mechanism, which provides the rate constants k_1 of the slow, continuous nucleation, P → Q, and k_2 of the autocatalytic surface growth, P + Q → 2Q for the formation of ruthenium(0) nanoparticles catalyst from the ruthenium(III) ions during the hydrolysis of ammonia borane (Table 3) [43]. Although it is not possible to get a direct correlation between the rate constant k_1 for nucleation and the catalyst concentration, the rate constant k_2 for surface growth decreases with the increasing concentration of ruthenium.

The hydrogen generation rate was determined from the linear portion of each plot in Fig. 8a and plotted versus the initial concentration of ruthenium, both in logarithmic scale, in Fig. 8b, which gives straight line with a slope of 0.95 indicating that the catalytic hydrolysis of AB is first order with respect to the ruthenium concentration.

The turnover frequency for hydrogen generation from the hydrolysis of AB (100 mM) at 25.0 ± 0.1 °C was determined from the hydrogen generation rate in the linear portion of plots given in Fig. 8a for experiments starting with 100 mM AB plus Ru(0)@HAp with a loading of 3.96 wt.% Ru. The TOF value of Ru(0)@HAp catalyst is as high as 137 min^{-1} (mol H_2/mol Ru min^{-1}) in the hydrolytic dehydrogenation of ammonia borane at 25.0 ± 0.1 °C. TOF values of the reported ruthenium catalysts used in hydrolytic dehydrogenation of ammonia borane are listed in Table 4 for comparison. As clearly seen from the comparison of values listed in

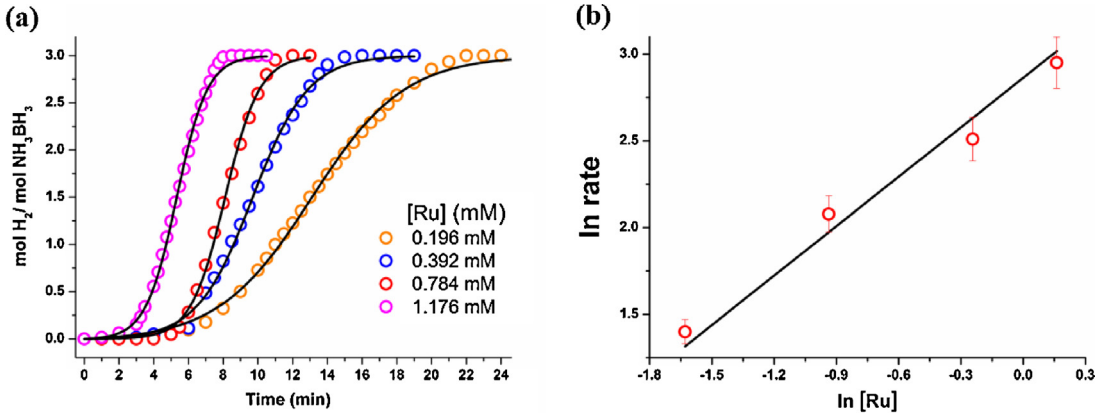

Fig. 8. (a) mol H_2/mol $H_3N{\cdot}BH_3$ versus time graph depending on the ruthenium concentration in Ru(0)@HAp for the hydrolysis of AB (100 mM) at 25.0 ± 0.1 °C. (b) The plot of hydrogen generation rate versus the concentration of Ru, both in logarithmic scale; ln(rate) = 0.95 ln[Ru] + 2.86.

Table 4
Catalytic activity of reported ruthenium catalysts used for the hydrolytic dehydrogenation of AB.

Entry	Catalyst	E_a (kJ/mol)	TOF (min^{-1})	Ref.
1	Ru/C	34.8	429.5	[51]
2	Ru(0)@MWCNT	33	329	[36]
3	Ru(0) NP/PSSA-co-MA	54	172	[52]
4	Ru(0)@HAp	58	137	This study
5	Ru/carbon	76	113	[47]
6	RuNPs@ZK-4	28	90.2	[48]
7	Ru@Al_2O_3	48	83.3	[49]
8	Ru(0) NP/laurate	47	75	[50]

Table 4, Ru(0)@HAp provide catalytic activity comparable to that of Ru/Carbon [47], RuNPs@ZK-4 [48], Ru@Al_2O_3 [49], Ru(0)NP/laurate [50] in hydrolytic dehydrogenation of AB. The high catalytic activity of Ru(0)@HAp can be attributed to the well dispersion of nanoparticles with a high accessible active sites on the nanoparticles surface. However, the catalytic activity of Ru(0)@HAp is lower than that of Ru(0)@MWCNTs [36], Ru/C [51], Ru(0)NP/PSSA-co-MA [52]. The lower activity of ruthenium(0) nanoparticles supported on hydroxyapatite compared to the carbon supported ones may be attributed to their larger particle size than that of the latter [53].

Activation energy for the hydrolytic dehydrogenation of ammonia borane catalyzed by Ru(0)@HAp could be determined by evaluating the temperature dependent kinetic data presented in Fig. 2a. The rate constants for the hydrogen generation at different temperature were calculated from the slope of linear portion of each plot given in Fig. 2a and used for the calculation of activation energy ($E_a = 58 \pm 2$ kJ/mol) from the Arrhenius plot in Fig. 9. The activation energy for the hydrolytic dehydrogenation of ammonia borane catalyzed by Ru(0)@HAp is comparable to the literature values reported for the other ruthenium catalysts in the same reaction (Table 4).

Reusability of Ru(0)@HAp catalyst was tested in successive experiments performed using the catalyst isolated from the reaction solution after a previous run of hydrolysis of AB. After the completion of hydrogen generation from the hydrolysis of AB starting with 0.567 mM Ru(III)@HAp plus 100 mM AB in 10 mL aqueous solution at 25.0 ± 0.1 °C, the catalyst was isolated by centrifugation, washing with water and drying under vacuum (10^{-3} Torr) at 80 °C. The whole powder materials were weighed and then redispersed in 10 mL solution containing 100 mM AB and a second run of hydrolysis was started immediately and continued until the completion of hydrogen evolution. This was repeated five times. Fig. 10 shows the percentage of initial catalytic activity of Ru(0)@HAp in the subsequent catalytic hydrolysis of 100 mM ammonia borane performed by using the catalyst isolated after the previous run of hydrolysis at 25.0 ± 0.1 °C. The material loss has already been taken into account in calculating the activity in each run during the isolation and redispersion processes.

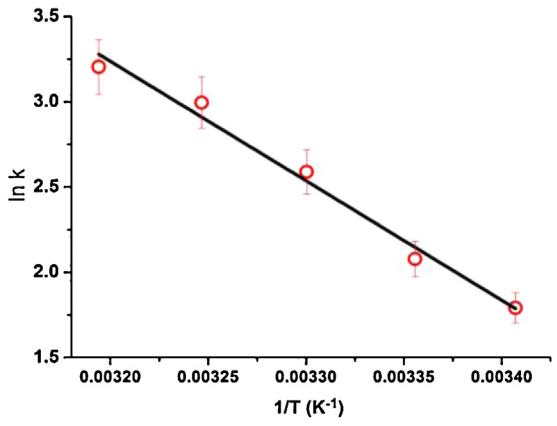

Fig. 9. The Arrhenius plot for the Ru(0)@HAp catalyzed hydrolytic dehydrogenation of AB ([$H_3N.BH_3$] = 100 mM and [Ru] = 0.392 mM). $ln k = -7004.83(1/T) + 25.65$.

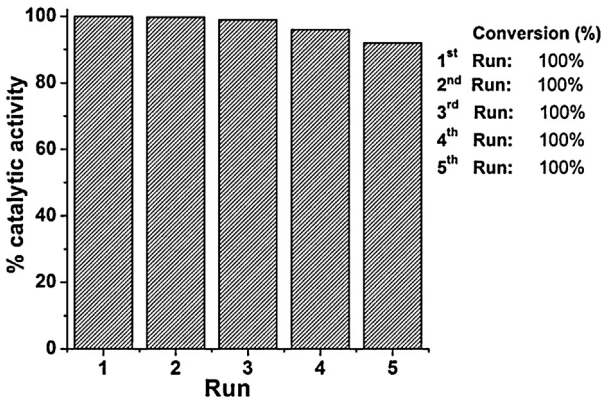

Fig. 10. The percentage of initial catalytic activity of Ru(0)@HAp ([Ru] = 0.567 mM) in successive runs after the reuse for the hydrolytic dehydrogenation of ammonia borane (100 mM).

The reusability tests reveal that Ru(0)@HAp are still active in the subsequent runs of hydrolytic dehydrogenation of AB providing 100% conversion, i.e. a release of 3.0 equivalent H_2 per mole of NH_3BH_3. After the fifth run hydrolytic dehydrogenation of AB, Ru(0)@HAp preserve 92% of their initial catalytic activity. As shown in Fig. 11, the Ru(0)@HAp have much higher reusability than most of the ruthenium(0) nanoparticles catalysts reported in the literature for the same reaction (Table 4). This comparison indicates that ruthenium(0) nanoparticles supported on hydroxyapatite can retain their high catalytic activity for a longer time than the other ruthenium catalysts given in Table 4. The importance of measuring the lifetime of catalyst is also implied by this observation.

Catalytic lifetime of Ru(0)@HAp was determined by measuring the total turnover number (TTO) in the hydrolysis of ammonia borane. A catalyst lifetime experiment was performed starting with 20 mg Ru(0)@HAp (ruthenium loading = 3.96 wt.% Ru, and [Ru] = 0.784 mM) in 100 mL solution of AB at 25.0 ± 0.1 °C. Fig. 12 shows the variation in turnover number (TON) and turnover frequency (TOF) in the course of reaction. The TOF value decreases expectedly as the ruthenium(0) nanoparticles catalysts are deactivated during the lifetime experiment. Ruthenium(0) nanoparticles supported on hydroxyapatite provide

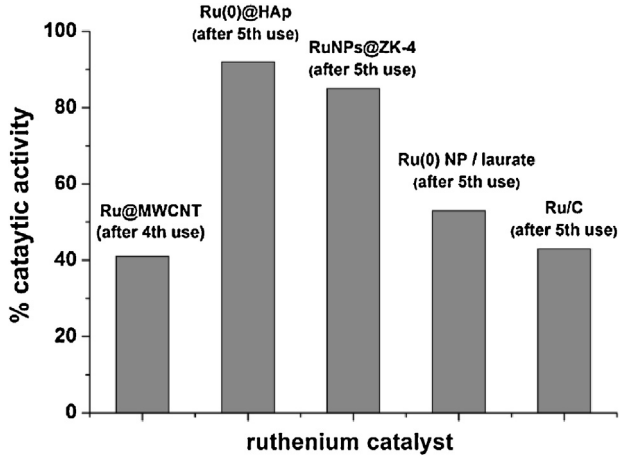

Fig. 11. The percentage of initial catalytic activity of various reported ruthenium catalysts after the reuse for the hydrolytic dehydrogenation ammonia borane. The literature values were obtained from the references cited in Table 4.

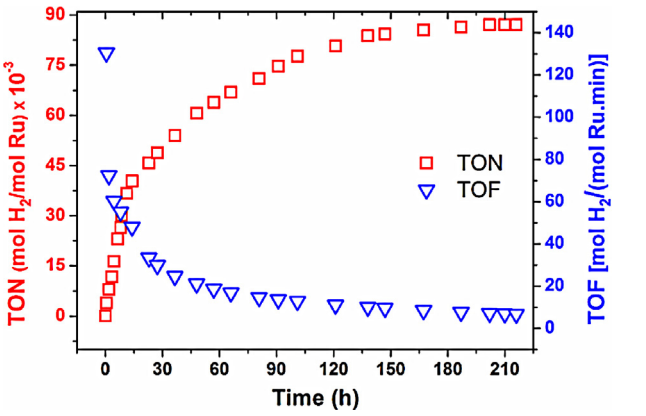

Fig. 12. The variation in turnover number (TON) and turnover frequency (TOF) during the catalytic lifetime experiment performed starting with 20 mg Ru(0)@HAp (ruthenium loading = 3.96 wt.% Ru, and [Ru] = 0.784 mM) in 100 mL solution of AB at 25.0 ± 0.1 °C.

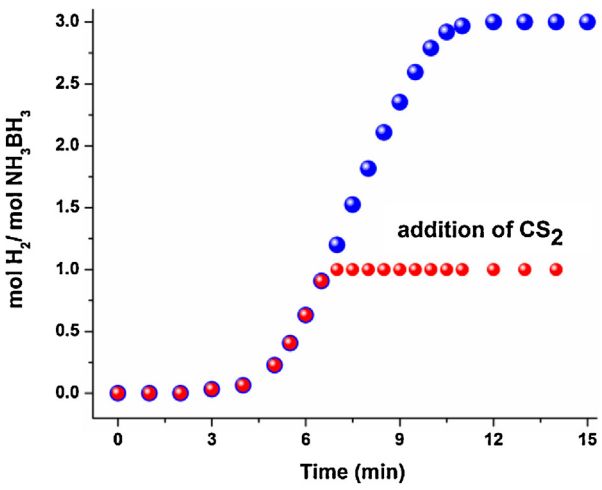

Fig. 14. The evolution of equivalent hydrogen per mole of AB versus time plot for the hydrolytic dehydrogenation of AB starting with Ru(III)@HAp precatalyst (0.784 mM Ru) and 100 mM AB with and without addition of CS_2 (0.157 mM) at 25.0 ± 0.1 °C.

minimum 87,000 turnovers over 202 h in the hydrolysis of AB at 25.0 ± 0.1 °C before deactivation of the catalyst. As shown in Fig. 13, Ru(0)@HAp provide the highest TTO value ever reported for the hydrolytic dehydrogenation of ammonia borane using ruthenium catalysts such as Ru(0)@MWCNT (TTO = 26,400) [36], Ru(0)NP/PSSA-co-MA (TTO = 51,720) [52], RuNPs@ZK-4 (TTO = 36,700) [48], Ru(0)NP/laurate (TTO = 5900) [50]. The TTO value of Ru(0)@HAp is even higher than that of laurate-stabilized rhodium(0) nanoparticels (TTO = 80,000) [54] and zeolite-confined rhodium(0) nanoparticles (TTO = 47,200) [55].

The heterogeneous nature of the catalytic hydrolysis was confirmed by a poisoning experiment performed by adding CS_2 into the reaction solution during the hydrolytic dehydrogenation of ammonia borane. After about 30% of conversion in a typical hydrolytic dehydrogenation experiment starting with 0.784 mM Ru at 25.0 ± 0.1 °C, 0.2 equivalents of CS_2 (0.157 mM) per mol of ruthenium was added into the reaction solution and the progress of reaction was followed by monitoring the H_2 volume, as shown in Fig. 14. The complete cease of the catalytic dehdyrogenation of AB upon addition of 0.2 equivalents of CS_2 is additional evidence that ruthenium(0) nanoparticles are the true catalyst in the hydrolysis of AB [56].

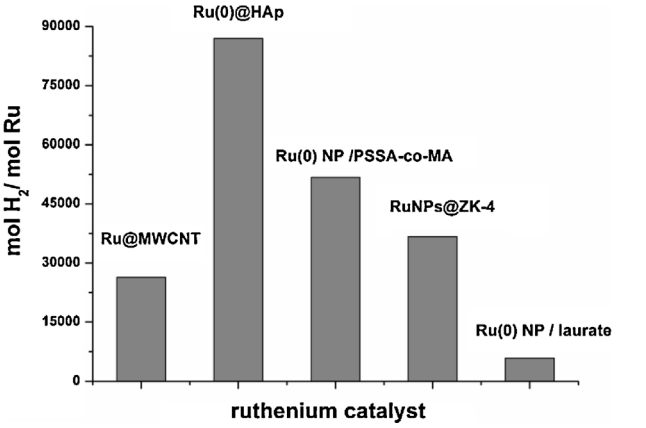

Fig. 13. Catalytic lifetime of reported ruthenium catalysts (TTO = mol H_2/mol Ru) in the hydrolytic dehydrogenation of ammonia borane. The literature values were obtained from the references cited in Table 4.

4. Conclusion

The main findings and conclusions from this work can be summarized as follows:

(1) The formation of ruthenium(0) nanoparticles supported on hydroxyapatite and the hydrogen generation from the hydrolysis of ammonia borane occur concomitantly in the same medium at room temperature.
(2) The use of hydrogen generation from the hydrolysis of ammonia borane as reporter reaction provides valuable insights to the formation kinetics of ruthenium(0) nanoparticles. All the kinetic data, collected for the nanoparticles formation and concomitant hydrolytic dehydrogenation of ammonia borane catalyzed by hydroxyapatite-supported ruthenium(0) nanoparticles under various experimental conditions, fit well to the 2-step mechanism for the nanoparticles formation: the nucleation (P → Q, rate constant k_1) and then autocatalytic surface growth (P + Q → 2Q, rate constant k_2). The large value of k_2/k_1 ratio is indicative of the high level kinetic control in the formation of ruthenium(0) nanoparticles from the reduction of the precursor ruthenium(III) ions on hydroxyapatite.
(3) For the first time, the activation energies for the slow nucleation and autocatalytic surface growth of metal(0) nanoparticles could be obtained from the evaluation of rate constants k_1 and k_2; E_a = 166 ± 7 kJ/mol for the nucleation and E_a = 59 ± 2 kJ/mol for the autocatalytic surface growth of ruthenium(0) nanoparticles.
(4) Highly dispersed ruthenium(0) nanoparticles with particle size 4.7 ± 0.7 nm, supported on hydroxyapatite, were reproducibly prepared from the reduction of ruthenium(III) ions on the surface of hydroxyapatite during the catalytic hydrolysis of ammonia borane. They could be isolated from the reaction solution by filtration and characterized by a combination of advanced analytical techniques.
(5) The hydroxyapatite-supported ruthenium(0) nanoparticles show high catalytic activity in hydrogen generation from the hydrolysis of ammonia borane providing a release of 3.0 equivalent of H_2 gas per mole of ammonia borane. They provide a turnover frequency value up to 137 min^{-1} at 25.0 ± 0.1 °C.
(6) The hydroxyapatite-supported ruthenium(0) nanoparticles are long lived and reusable catalyst providing 87,000 turnovers for hydrogen generation from the hydrolysis of ammonia borane

and maintaining 92% of their initial catalytic activity even after the fifth run of hydrolysis of ammonia borane at 25.0 ± 0.1 °C.

(7) The results of quantitative kinetic study on the hydrogen generation from the hydrolysis of ammonia borane show that the hydrolytic dehydrogenation of ammonia borane is first order in ruthenium concentration and the activation energy is 58 ± 2 kJ/mol for the hydrolytic dehydrogenation of ammonia borane catalyzed by ruthenium(0) nanoparticles supported on hydroxyapatite.

Acknowledgements

Partial support by Turkish Academy of Sciences (TUBA) is gratefully acknowledged. We would like to thank Seçkin Öztürk and İlker Yıldız for TEM and XPS analyses, respectively.

References

[1] U. Eberle, M.F. Felderhoff, Schüth Angewandte Chemie Internationa Edition 48 (2009) 6608–6630.
[2] J. Turner, G. Sverdrup, K. Mann, P.G. Mannes, V. Kroposki, M. Ghirardi, International Journal of Hydrogen Energy 32 (2008) 379–407.
[3] A.W.C.V. Berg, C.O. Arean, Chemical Communications 6 (2008) 668–681.
[4] Basic research needs for the hydrogen economy, report of the basic energy sciences workshop on hydrogen production, storage, and use, May 13–15, 2003, Office of Science, U.S. Department of Energy, http://science.energy.gov/~/media/bes/pdf/reports/files/nhe_rpt.pdf
[5] J.M. Ogden, International Journal of Hydrogen Energy 24 (1999) 709–730.
[6] L. Schlapbach, A. Züttel, Nature 414 (2001) 353–358.
[7] A. Züttel, Materials Today 6 (2003) 24–33.
[8] A.M. Seayad, D.M. Antonelli, Advanced Materials 16 (2004) 765–777.
[9] R. Basca, C. Laurent, R. Morishima, H. Suzuki, M. Lelay, Journal of Physical Chemistry B 108 (2004) 12718–12723.
[10] M. Yadav, Q. Xu, Energy & Environmental Science 5 (2012) 9698–9725.
[11] Z.H. Lu, Q. Xu, Functional Materials Letters 5 (2012) 1230001–1230009.
[12] M. Chandra, Q. Xu, Journal of Power Sources 156 (2006) 190–194.
[13] M. Chandra, Q. Xu, Journal of Power Sources 159 (2006) 855–860.
[14] Q. Xu, M. Chandra, Journal of Power Sources 163 (2006) 364–370.
[15] M. Zahmakiran, F. Durap, S. Özkar, International Journal of Hydrogen Energy 35 (2010) 187–197.
[16] S. Çalışkan, M. Zahmakiran, S. Özkar, Applied Catalysis B: Environmental 93 (2009) 387–394.
[17] J.M. Yan, X.B. Zhang, S. Han, H. Shioyama, Q. Xu, Inorganic Chemistry 48 (2009) 7389–7393.
[18] Y. Yamada, K. Yano, Q. Xu, S. Fukuzumi, Journal of Physical Chemistry C 114 (2010) 16456–16462.
[19] J.M. Yan, X.B. Zhang, T. Akita, M. Haruta, Q. Xu, Journal of the American Chemical Society 132 (2010) 5326–5327.
[20] C.W. Hamilton, R.T. Baker, A. Staubitz, I. Manners, Chemical Society Reviews 38 (2009) 279–293.
[21] R.J. Keaton, M.J. Blacquiere, R.T. Baker, Journal of the American Chemical Society 129 (2007) 1844–1845.
[22] M.E. Bluhn, M.G. Bradley, R. Butterick III, U. Kusari, L.G. Sneddon, Journal of the American Chemical Society 128 (2006) 7748–7749.
[23] J.T. Clark, G.R. Whittell, I. Manners, Inorganic Chemistry 46 (2007) 7522–7527.
[24] M. Ramzan, F. Silvearv, A. Blomqvist, R.H. Scheicher, R.S. Lebeque, R. Ahuja, Physical Review B 79 (2009) 32102–132104.
[25] H. Erdogan, Ö. Metin, S. Özkar, Physical Chemistry Chemical Physics 11 (2009) 10519–10525.
[26] M. Zahmakiran, S. Özkar, Nanoscale 3 (2011) 3462–3481.
[27] X. Yang, F. Cheng, J. Liang, Z. Tao, J. Chen, International Journal of Hydrogen Energy 36 (2011) 1984–1990.
[28] X. Wang, D. Liu, S. Song, H. Zhang, Chemical Communications 48 (2012) 10207–10209.
[29] P. Xi, F. Chen, G. Xie, C. Ma, H. Liu, C. Shao, J. Wang, Z. Xu, X. Xu, Z. Zeng, Nanoscale 4 (2012) 5597–5601.
[30] G.P. Rachiero, U.B. Demirci, P. Miele, Catalysis Today 170 (2011) 85–92.
[31] S. Basu, A. Brockman, P. Gagare, Y. Zhen, P.V. Ramachandran, W.N. Delgass, Journal of Power Sources 188 (2009) 238–243.
[32] S. Özkar, R.G. Finke, Journal of the American Chemical Society 124 (2002) 5796–5810.
[33] S. Özkar, R.G. Finke, Langmuir 18 (2002) 7653–7662.
[34] M. Zahmakiran, S. Akbayrak, T. Kodaira, S. Özkar, Dalton Transactions 39 (2010) 7521–7527.
[35] M. Zahmakiran, T. Ayvalı, S. Akbayrak, S. Çalışkan, D. Celik, S. Ozkar, Catalysis Today 170 (2011) 76–84.
[36] S. Akbayrak, S. Özkar, ACS Applied Materials & Interfaces 4 (2012) 6302–6310.
[37] J. Wang, Y.L. Qin, X. Liu, X.B. Zhang, Journal of Materials Chemistry 22 (2012) 12468.
[38] M. Zahmakiran, Y. Tonbul, S. Özkar, Chemical Communications 46 (2010) 4788–4790.
[39] A.B. Lowe, B.S. Sumerlin, M.S. Donovan, C.L. McCormick, Journal of the American Chemical Society 124 (2002) 11562–11563.
[40] K. Kaneda, T. Mizugaki, Energy & Environmental Science 2 (2009) 655–673.
[41] M.A. Watzky, R.G. Finke, Journal of the American Chemical Society 119 (1997) 10382–10400.
[42] J.A. Widegren, J.D. Aiken, S. Ozkar, R.G. Finke, Chemistry of Materials 13 (2001) 312–324.
[43] M.A. Watzky, R.G. Finke, Chemistry of Materials 9 (1997) 3083–3095.
[44] M. Rakap, S. Özkar, Catalysis Today 183 (2012) 17–25.
[45] C. Wagner, G.E. Muilenber, W.M. Riggs, L.E. Davis, J.F. Moulder, Handbook of X-ray Photoelectron Spectroscopy, vol. 55, Perkin-Elmer, Physical Electronic Division, Eden Prairie, MN, 1979.
[46] Ö. Metin, S. Ozkar, International Journal of Hydrogen Energy 36 (2011) 1424–1432.
[47] S. Basu, A. Brockman, P. Gagare, Y. Zheng, P.V. Ramachandran, W.N. Delgass, J.P. Gore, Journal of Power Sources 188 (2009) 238–243.
[48] M. Zahmakiran, Materials Science and Engineering B 177 (2012) 606–613.
[49] H. Can, Ö. Metin, Applied Catalysis B: Environmental 125 (2012) 304–310.
[50] F. Durap, M. Zahmakiran, S. Ozkar, International Journal of Hydrogen Energy 34 (2009) 7223–7230.
[51] H. Liang, G. Chen, S. Desinan, R. Rosei, F. Rosei, D. Ma, International Journal of Hydrogen Energy 3 (2012) 17921–17927.
[52] Ö. Metin, Ş. Sahin, S. Ozkar, International Journal of Hydrogen Energy (2009) 6304–6313.
[53] D. Sun, V. Mazumder, Ö. Metin, ACS Nano 5 (2011) 6458–6464.
[54] F. Durap, M.S. Zahmakiran, Ozkar Applied Catalysis B: General 369 (2009) 53–59.
[55] M. Zahmakiran, S. Ozkar, Applied Catalysis B: Environmental 89 (2009) 104–110.
[56] B.J. Hornstein, J.D. Aiken, R.G. Finke, Inorganic Chemistry 41 (2002) 1625.